Infant Skull and Suture Properties: Measurements and Implications for Mechanisms of Pediatric Brain Injury

Susan S. Margulies
e-mail: margulies@seas.upenn.edu

Kirk L. Thibault

Department of Bioengineering,
University of Pennsylvania,
Philadelphia, PA 19104

*The mechanical properties of the adult human skull are well documented, but little information is available for the infant skull. To determine the age-dependent changes in skull properties, we tested human and porcine infant cranial bone in three-point bending. The measurement of elastic modulus in the human and porcine infant cranial bone agrees with and extends previous published data [McPherson, G. K., and Kriewall, T. J. (1980), J. Biomech., **13**, pp. 9–16] for human infant cranial bone. After confirming that the porcine and human cranial bone properties were comparable, additional tensile and three-point bending studies were conducted on porcine cranial bone and suture. Comparisons of the porcine infant data with previously published adult human data demonstrate that the elastic modulus, ultimate stress, and energy absorbed to failure increase, and the ultimate strain decreases with age for cranial bone. Likewise, we conclude that the elastic modulus, ultimate stress, and energy absorbed to failure increase with age for sutures. We constructed two finite element models of an idealized one-month old infant head, one with pediatric and the other adult skull properties, and subjected them to impact loading to investigate the contribution of the cranial bone properties on the intracranial tissue deformation pattern. The computational simulations demonstrate that the comparatively compliant skull and membranous suture properties of the infant brain case are associated with large cranial shape changes, and a more diffuse pattern of brain distortion than when the skull takes on adult properties. These studies are a fundamental initial step in predicting the unique mechanical response of the pediatric skull to traumatic loads associated with head injury and, thus, for defining head injury thresholds for children.* [S0148-0731(00)00904-3]

Introduction

The response of the head to traumatic loading is intrinsically linked to the anatomy and mechanical properties of the developing skull/brain structure. The skull of the newborn consists of thin, flexible plates composed of partially calcified bony tissue joined at their margins by patent, membranous sutures. In contrast to the stiff adult cranium, the infant skull is a compliant structure capable of substantial deformation under external loading.

Previous studies have reported the quasi-static elastic modulus of cranial bone [1,2] and the structural stiffness of fetal parietal bone [3] but have not characterized the cranial sutures. However, there is a paucity of dynamic mechanical property data for the tissues constituting the infant brain case. Therefore, previous biomechanical studies of traumatic pediatric head injury [4–7] have neglected the role of the skull when determining the mechanical response of the pediatric head to trauma, or have relied on qualitative approximations of its mechanical properties.

The aim of this paper is to define the mechanical properties of the developing skull and sutures and to demonstrate their influence in the biomechanical response of the infant brain case to impact loading. We report our results from a series of mechanical tests on cranial bone from infant humans, and cranial bone and suture from infant pigs. Specifically, we define the dynamic properties of human infant cranial bone, correlate the mechanical behavior of human infant cranial bone with porcine infant cranial bone, and extend the results of the human cranial bone tests with the porcine data.

As a first-order demonstration of the influence that these age-dependent mechanical properties of cranial bone and suture have in protecting the infant brain from deformation during an impact, an idealized finite element model of the infant head was constructed. Two models were constructed, a first with infant cortical bone and suture properties determined in the present study, and a second with adult cortical bone and suture properties obtained from the literature. The two model formulations were exposed to identical loads, and the intracranial strains were compared. Together, the experimental and computational studies reported in this communication provide a foundation for predicting the unique mechanical response of the pediatric skull to traumatic loads applied to the head.

Contributed by the Bioengineering Division for publication in the JOURNAL OF BIOMECHANICAL ENGINEERING. Manuscript received by the Bioengineering Division: January 7, 1999; revised manuscript received March 28, 2000. Associate Technical Editor: R. C. Haut.

Methods

Human Infant Cranial Bone: Harvest and Sample Preparation. Human infant cranial bone specimens were obtained at autopsy ($N=4$ subjects) from the morgue at the Children's Hospital of Philadelphia under the approval of the Institutional Review Board (IRB) for human subject research. Subjects ranged from 25 weeks gestation to six months of age and were free from any craniofacial surgical procedures or injuries to the head. For each subject, age, sex, date of death, and cause of death were recorded. Due to standard autopsy procedures for removing the brain en bloc, no suture material could be collected from these subjects. Bilateral strips of parietal bone adjacent to the sagittal suture were excised and placed in a sealed container over a saline-soaked gauze pad. The strips were then frozen at −4°C until preparation for testing.

To determine the age-related properties of cranial bone independent of any inherent anisotropy or inhomogeneity, all beam-shaped specimens were cut from the parietal bone *parallel* to the sagittal suture (Fig. 1) at room temperature, and the location and

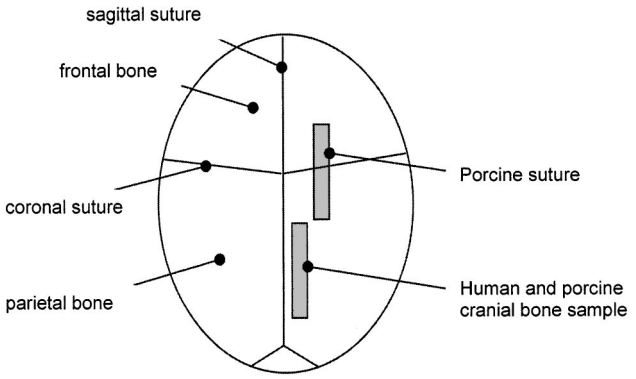

Fig. 1 Infant cranial vault: Shaded areas represent approximate size and location of skull and suture samples removed.

orientation of the samples remained constant across all subjects. Test specimens were typically 3–5 mm wide and 20–25 mm long, depending upon the size of the original donor sample. All specimens were cut with a diamond-coated cutting wheel (Stoelting Co., Wood Dale, IL) mounted in a variable-speed Dremel Moto-Tool (Dremel, Racine, WI) under a constant drip of saline. Test specimens were refrozen at −4°C until testing.

Porcine Cranial Bone and Suture: Harvest and Sample Preparation. Neonate pigs (age 2–3 days, $N=30$) were sacrificed by a lethal injection of KCl as detailed in experimental protocols approved by the Animal Care and Use Committee of the University of Pennsylvania. Time of death and age were recorded for each animal immediately post-mortem. The cranial vault of each animal was excised and frozen at −4°C until preparation for testing. Samples were randomized with respect to right or left side but the location and orientation of the samples remained constant across all studies.

Infant Cranial Bone and Suture: Three-Point Bending Specimens. The left or right side frontoparietal bones from excised cranial vaults from 20 of the 30 infant pigs were prepared for testing in three-point bending to failure. Beam-shaped test specimens of parietal bone alone and frontoparietal bone with a portion of coronal suture penetrating the cross section of the beam were cut from the cranial vault parallel to the sagittal suture (Fig. 1). Porcine specimen preparation and storage was identical to that for the human.

Infant Cranial Bone and Suture: Tension Specimens. The left or right side frontoparietal bones from excised cranial vaults of the remaining 10 infant pigs were prepared for testing in tension to failure. Rectangular prismatic ''blanks'' of cranial bone or cranial bone with a portion of coronal suture penetrating the cross section of the sample were prepared as described previously for three-point bending samples. Each blank was machined to the tensile testing configuration with a typical gage section of 3–5 mm wide and 8–11 mm long. Tensile specimens were shaped with an aluminum oxide grinding wheel mounted in a variable-speed Dremel Moto-Tool under a constant drip of saline. The ends of each machined specimen were potted in polymethylmethacrylate (PMMA, Hygenic Corp., Akron, OH) to facilitate gripping of the specimen without crushing it.

Care was taken to ensure that the potential for the sample to slip within the PMMA blocks during testing was reduced by machining a sloping profile in the embedded portion of the tissue sample. Slippage of the sample within the grips or the PMMA blocks was monitored carefully during each test and was identified as a region of constant force on a force-displacement curve. Three of the infant test specimens exhibited slippage within the PMMA blocks, and were eliminated from analysis.

Three-Point Bending Test Protocol. Samples of cranial bone and suture were tested in three-point bending on a custom-designed fixture with an adjustable span (10–300 mm) built for an Instron servohydraulic materials testing machine (Instron Corp., Canton, MA). A stainless steel loading nose and supports with a radius of 3.2 mm support were used to avoid excessive indentation and stress concentrations within the specimen (ASTM D 790-98). Three-point bending is suitable for ultimate strains less than or equal to 5 percent, and four-point bending for larger ultimate strains (ASTM D 790-98). Ultimate strain data (determined in tension) presented in Table 3 show that skull properties are well within the accepted range, and suture ultimate strains (averaging 6 percent) are slightly higher than the accepted limit for three-point bending tests. Centerline deflection of the specimen was determined from the displacement of the servohydraulic actuator, and force was measured with a 50 lb isometric load cell (Interface, Inc., Scottsdale, AZ). Centerline deflection and force data were recorded via a PC-based, digital data acquisition system (National Instruments, Austin, TX) as well as an $X-Y$ recorder (Hewlett Packard, Loveland, CO) for hardcopy backup.

Bone samples were warmed to room temperature in a bath of saline, placed on the bending fixture in a manner consistent with simply supported boundary conditions and loaded midspan. Each constant rate bending test to failure was performed at 2.54 mm/min or 2540 mm/min while centerline deflection, as measured by the displacement of the servohydraulic actuator, and force were recorded. All tests were conducted at ambient room temperature (25°C). A constant span of 17 mm was used for all skull samples (human and porcine) except for the samples from the six-month-old human subject, which could accommodate a span of 30 mm. In all tests, failure occurred directly under the point of load, on the tensile face of the beam, and the width and depth of each specimen were measured directly adjacent to this point.

Tension Test Protocol. A custom-designed set of tensile test grips was designed for use with an Instron servohydraulic materials testing machine (Instron Corp.). The ends of the tensile test specimen embedded in PMMA were placed in the brass collet grips, and an extensometer (Instron Corp.) fastened to each of the PMMA blocks with elastic bands measured the strain in the sample. Because excessive vibration was encountered while measuring low forces at the higher loading rate in tension, data from infant porcine cranial bone with and without sutures was obtained in tension at 2.54 mm/min only.

Extensometer displacement and force were recorded as described earlier for three-point bending. The displacement within the system was assumed to occur entirely within the gage section of the tissue sample. The gage length of each undeformed specimen was measured prior to testing, and the width and thickness of each test specimen were measured adjacent to the cross section where fracture occurred. All samples failed within the gage section.

Idealized Finite Element Model Development. A finite element model of an idealized one-month-old infant head was constructed using ANSYS 5.3 (ANSYS Inc., Houston, PA). The model consisted of a rigid impactor plate, and a skull/brain with five regions: the cranial bone of the skull, the sutures, the anterior fontanel, the foramen magnum, and the brain (Fig. 2). The contact problem was solved using LS-DYNA3D's automatic surface-to-surface contact formulation (LSTC, Livermore, CA). The model consisted of 12,772 elements and 11,823 nodes, and a zoning study was performed to verify convergence. The cranial bone, suture, fontanel, and foramen magnum were modeled using four-noded linear shell elements. The brain and impactor were modeled using eight-noded linear brick elements.

Two formulations, one using an infant cranial bone and another using adult cranial bone representations, were constructed with the same geometry, boundary conditions, brain properties, and loading conditions, differing only in the braincase material prop-

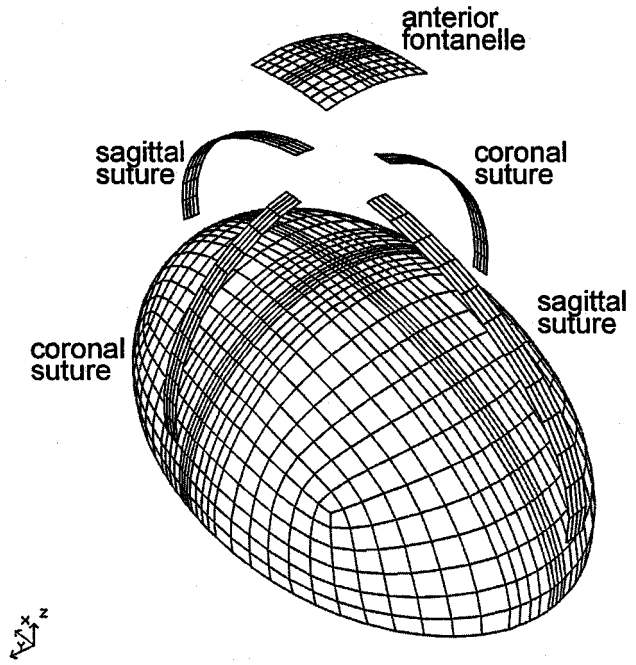

Fig. 2 Schematic of finite element mesh. Refer to text for skull and suture properties.

erties. The ''infant'' formulation was assigned pediatric material properties for the cranial bone and suture in the range of those reported in Tables 1–3 and Kriewall [3]. In the ''adult'' formulation the sutures were assumed to be completely fused, having properties similar to adult human cranial bone [8,9]. Skull material properties are listed in Table 4.

Brain material properties were based on experimentally determined mechanical response of infant porcine brain tissue [10]. The brain was represented as a linear viscoelastic solid

$$G(t)=G_\infty+(G_0-G_\infty)e^{-\beta t} \tag{7}$$

where $G_\infty=2.32\times10^{-3}$ MPa, $G_0=5.99\times10^{-3}$ MPa, and $\beta=0.09248$ s. The brain was assumed incompressible with a bulk modulus of 2110 MPa. The elastic modulus of the foramen magnum was chosen as 100 MPa to simulate the mechanical impedance of the spinal cord to brainstem herniation.

The base of the cranial vault was fixed to simulate pure impact loading with no rotation or translation of the head following impact. The brain and skull were assumed to be displacement compatible, with no slip at the interface between the two materials.

The impact loading conditions were based on accelerations measured by Duhaime et al. [5] in a biomechanical study of shaken impact syndrome. Half-sinusoidal load-time histories with a 10 ms pulse duration and peak magnitudes of 1000 N and 5000 N were selected to simulate minor and severe impact loads, respectively. Loads were applied to the parietal region of the skull at 45 deg relative to the vertical axis.

Table 1 Mechanical properties of human infant cranial bone in three-point bending

Case	Age	Sample	Location	Rate (mm/min)	σ_{rupt} (MPa)	E (MPa)	U_o (N.mm/mm^3)
1	25 wks gest.	1	L Parietal	2.54	4.5	71.6	0.0312
		2	L Parietal	2540	4.0	43.8	–
2	30 wks gest.	1	L Parietal	2.54	3.1	95.3	
		2	R Parietal	2540	11.2	444.5	0.0624
		3	R Parietal	2.54	14.9	618.8	
		4	R Parietal	2540	8.9	407.7	0.0575
		5	R Parietal	2540	17.0	455.4	0.0675
3	1 wk term	1	L Parietal	2540	10.6	820.9	0.0607
4	6 mos term	1	L Parietal	2.54	42.1	2111.7	0.1392
		2	R Parietal	2.54	44.6	2199.4	0.1834
		3	L Parietal	2540	NR**	2671.9	NR**
		4	R Parietal	2540	71.7	3582.2	0.4361

The mechanical properties of infant cranial bone for the four subjects tested in three-point bending. **These values are not reported because the final portion of the stress-strain curve was off-scale.

Table 2 Bending properties of porcine infant bone and suture

	σ_{rupt} (MPa)	E (MPa)	U_o (N.mm/mm3)
Cranial Bone - Slow (n=11)			
mean	17.4	615.0	0.1009
stand. error	2.1	96.2	0.0182
Cranial Bone - Fast (n=13)			
mean	41.4	1371.4	0.1688
stand. error	6.6	275.8	0.0338
Suture - Slow (n=6)			
mean	12.4	194.2	0.1127
stand. error	2.7	42.5	0.0327
Suture - Fast (n=7)			
mean	30.8	610.3	0.1737
stand. error	5.1	122.6	0.0415

Mean value and standard error of bending properties for porcine infant cranial bone and suture at slow (2.54 mm/min) and fast (2540 mm/min) loading rates

Data Analysis

Three-Point Bending Test Analysis. For each test specimen, the rupture modulus (σ_{rupt}), elastic modulus (E), and energy per unit volume absorbed to failure (U_0) were calculated from the measured force and centerline deflection data. Samples of cranial bone with and without sutures were analyzed identically. The maximum bending stress was calculated using simple beam theory for rectangular cross sections, modified for a midspan point according to the expression [11]

$$\sigma_{rupt}=\frac{3P_{max}}{2c^3}\left(\frac{L}{4}-\frac{c}{\pi}\right)c-0.133\left(\frac{P_{max}}{c}\right) \tag{1}$$

where σ_{rupt} is the rupture modulus, P_{max} is the maximum force per unit width of the beam, c is the half-depth of the beam, and L is the span. This formulation of bending stress applies exclusively to the point on the tensile surface of the beam directly under the applied load, where failure is most likely to occur [8]. In every bending test, we observed failure at this location.

Elastic modulus was calculated using beam theory according to the relationship

$$E=\left(\frac{F}{\omega}\right)\frac{L^3}{48I} \tag{2}$$

where F is the measured force, ω is the centerline deflection, L is the span of the beam, and I is the moment of inertia of the beam's rectangular cross section. The linear elastic portion of the force-deflection curve was fit with a linear regression to obtain the quantity F/ω used in Eq. (2).

Energy absorbed to failure was calculated by

$$U_0=\frac{\int F\cdot d\omega}{V} \tag{3}$$

and computed by integrating the digital force-deflection curve with a simple trapezoid rule scheme and dividing by the volume, V, of the sample (width×depth×span).

Tensile Test Analysis. For each test specimen, ultimate stress and yield stress (σ_{ult},σ_y), ultimate strain and yield strain (ε_{ult},ε_y), elastic modulus (E), and energy per unit volume absorbed to failure (U_0) were calculated from the measured force

Table 3 Comparison of tensile properties of porcine infant bone and suture

	σ_{yield} MPa	σ_{ult} MPa	ε_{yield} mm/mm	ε_{ult} mm/mm	E MPa	U_0 N.mm/mm3
*p ≤ 0.05	-	-	*	*	*	-
Bone (n=6)						
mean	5.3	10.6	0.0079	0.0341	809.0	0.0075
stand. error	0.9	1.6	0.0010	0.0069	118.9	0.0022
Suture (n=3)						
mean	5.7	7.7	0.0422	0.0664	171.5	0.0033
stand. error	0.9	0.8	0.0040	0.0078	32.5	0.0005

Results from Student's t Test for porcine infant cranial bone and suture tested in tension. A significant difference between bone and suture at the level of p≤0.05 is indicated by *. Also listed are the mean values and standard errors for each property. All tests were at the slow (2.54 mm/min) loading rate.

(F) and displacement (δ) data. Samples of cranial bone with and without suture were analyzed identically. In this analysis it was assumed that ''necking'' or ''drawing'' of the gage section of the tensile specimens was negligible, and engineering stress and Lagrangian strain were used exclusively. Stress, σ, was defined as

$$\sigma = \frac{F}{A_0} \tag{4}$$

where A_0 is the original cross-sectional area of the specimen. Strain, ε, was defined as

$$\varepsilon = \frac{\delta}{L_0} \tag{5}$$

where L_0 is the initial gage length of the specimen. The ultimate stress, σ_{ult}, was defined as the maximum stress during the experiment and the ultimate strain, ε_{ult}, was defined as the strain corresponding to σ_{ult}.

The elastic modulus, E, was defined as the slope of the linear regression ($\sigma = E\varepsilon$) in elastic regime of the stress–strain curve. Because infant cranial bone and suture are capable of large plastic deformations, the typical 0.2 percent offset yield criterion was not used in this analysis to define σ_y and ε_y. A power law plastic behavior characterization proposed by Datsko [12] was fit to the plastic regime of the stress–strain curve using the equation

$$\sigma = \sigma_0 \varepsilon^m \tag{6}$$

where σ_0 is called the ''strain-strengthening coefficient,'' ε is the plastic strain, and m is called the ''strain-strengthening exponent.'' Yield strain, ε_{yield}, for the elastic–plastic material was defined as the intersection of the plastic regime power law curve ($\sigma = \sigma_0 \varepsilon^m$) and the linear elastic regime regression line ($\sigma = E\varepsilon$) [12]. Yield strain was determined with a numerical optimization routine (Microsoft Excel Solver, Microsoft Corp). The yield stress, σ_{yield}, was defined as the measured value of stress on the experimental stress–strain curve associated with the calculated ε_{yield} (Fig. 3). Energy absorbed to failure was obtained from Eq. (3), replacing deflection ω with displacement δ.

Table 4 Physical and material properties of finite element skull models

Material	Model	E (MPa)	ρ kg/m³	ν
Cranial Bone	infant	1300	2150	0.28
	adult	10000	2150	0.28
Suture	infant	200	1130	0.28
	adult	10000	2150	0.28

Results

Human Infant Cranial Bone. Rupture modulus, elastic modulus, and energy absorbed to failure were evaluated for human infant cranial bone samples in three-point bending ($N=4$ subjects, 12 samples total) at ''slow'' (2.54 mm/min) and ''fast'' (2540 mm/min) rates as listed in Table 1. The age given in Table 1 is based on a term pregnancy of 40 weeks; thus the age of a premature subject is listed as ''gestational age'' and the age of a term subject is listed as ''term'' age, or age after birth.

The rupture modulus, elastic modulus, and energy absorbed to failure for both loading rates are plotted as a function of age in Figs. 4(a)–(c), respectively. Unlike the age convention in Table 1, the abscissa of all plots is in continuous weeks' of age, with 40 weeks representing birth. Due to the small number of samples tested, few statistical conclusions may be drawn from these data, including a statistical analysis of rate dependence. However, all three parameters measured show an increase in their respective magnitudes as a function of age. This increase appears to take place between birth and six months of age. It may be argued that increases in rupture modulus and elastic modulus also occur between 25 weeks gestation and birth, but the data are inconclusive.

Porcine Infant Cranial Bone and Suture. Porcine skull testing complemented and extended the human data, and allowed for

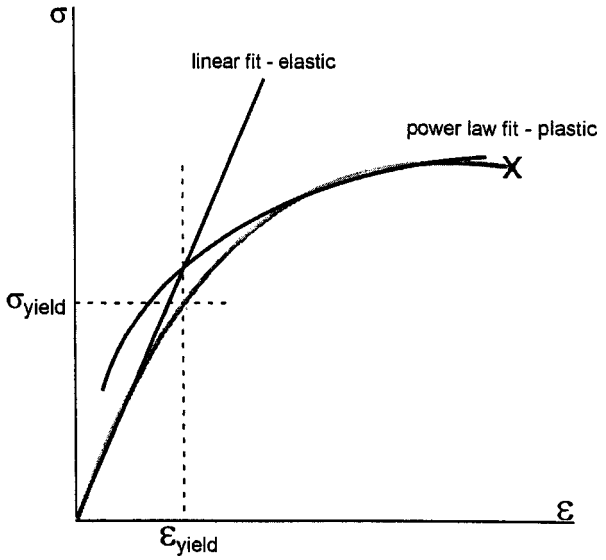

Fig. 3 Schematic diagram of yield criteria for tensile tests

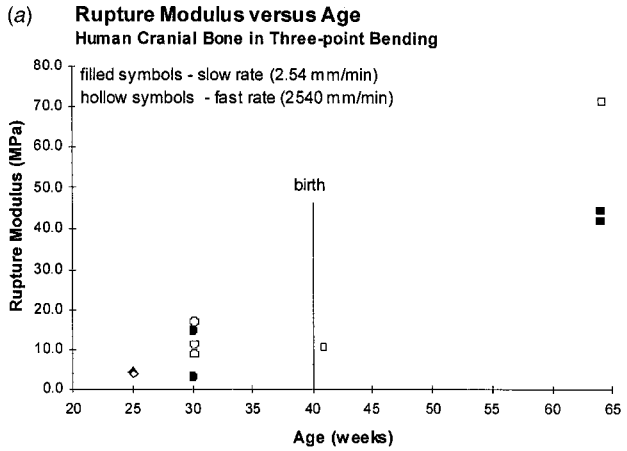

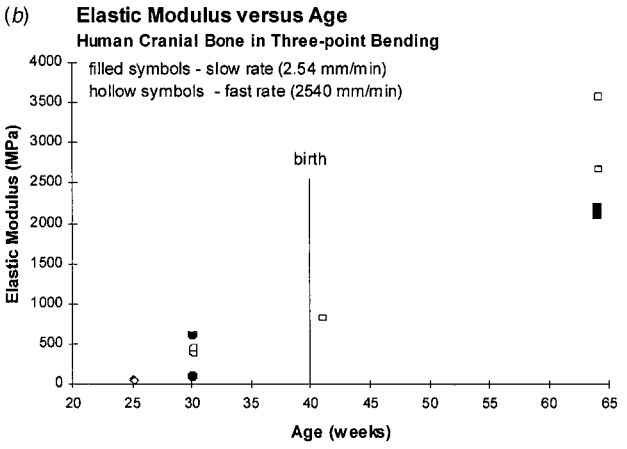

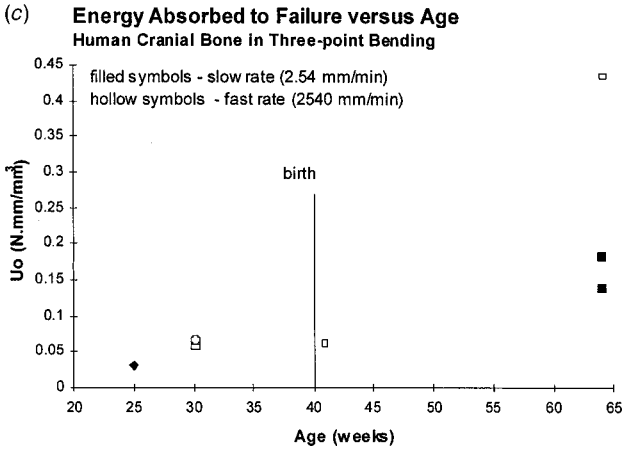

Fig. 4 Human infant cranial bone specimens: (*a*) rupture modulus, (*b*) elastic modulus, and (*c*) energy absorbed to failure plotted against age

more extensive analysis of the rate dependence of bone and suture. The mechanical property data measured for the infant porcine cranial bone are presented in two portions: results from three-point bending tests and results from tensile tests.

Three-Point Bending Test Results. The elastic modulus, rupture modulus, and energy absorbed to failure were determined for porcine cranial bone and suture at slow (2.54 mm/min) and fast (2540 mm/min) loading rates. Table 2 lists the mean and standard error of the bending properties of porcine infant cranial bone and suture for slow and fast loading rates. The data were arranged into

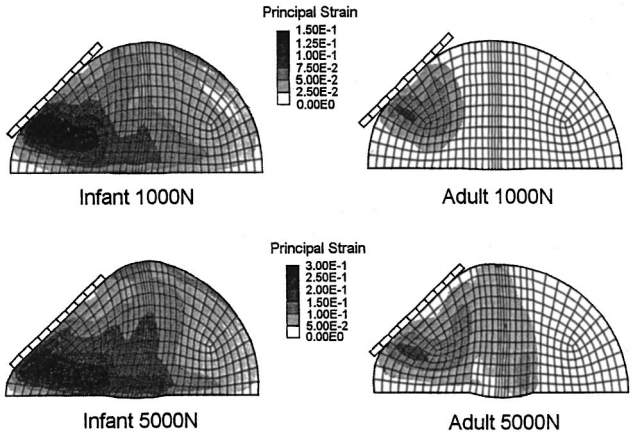

Fig. 5 Maximum principal strain in idealized infant head finite element model at $t=5$ ms (at peak load) for adult braincase properties and pediatric properties, for half-sine load magnitudes of 1000 N and 5000 N, respectively

four groups for parametric analysis to facilitate analysis of differences in mechanical behavior between tissue types (bone versus suture) and rates (slow versus fast). A two-tailed Student's *t*-test assuming unequal variances was used to determine whether a significant difference existed between each pair of corresponding mean values at the level of $p \leq 0.05$. The elastic modulus of bone was significantly greater than suture at both loading rates. The rupture modulus and energy absorbed to failure were not significantly different between bone and suture at either loading rate. The comparison between fast and slow loading rates revealed that loading rate significantly affected the rupture modulus and elastic modulus. The rupture modulus and elastic modulus of both bone and suture were significantly greater at the fast loading rate than at the slow loading rate. The energy absorbed to failure in pediatric bone and suture was not significantly affected by loading rate.

Tensile Test Results. The results of the tensile tests of porcine infant cranial bone and suture at 2.54 mm/min are presented in Table 3. Significant differences ($p \leq 0.5$, using two-tailed Student's *t*-test assuming unequal variances) between bone and suture were found in the yield strain, ultimate strain, and elastic modulus. The yield stress, ultimate stress, and energy absorbed to failure were not significantly different between bone and suture. These results are consistent with the findings from the three-point bending tests; however, only the value of energy absorbed to failure in tension was statistically similar to bending ($p > 0.05$) at the slow loading rate. The disparity between the elastic modulus in bending and in tension is most likely due to the differences in test methods and analysis. Specifically, the bending analysis relies on beam theory to calculate the modulus whereas the tensile test measures the modulus directly. Likewise, the maximum stress in a bending test (rupture modulus) is calculated from beam theory, whereas the maximum stress in a tensile test (ultimate stress) is measured directly.

Idealized Finite Element Model Results. The deformation of the braincase and the resulting intracranial strains were highly sensitive to the properties of the cranial vault (Fig. 5). The peak intrusion of the impactor was more than 100 percent greater in the simulation with the infant cranial bone representation than that with the adult (4 versus 2 mm, and 10 versus 4 mm for the 1000 and 5000 N loads, respectively). Furthermore, impact loading to the infant braincase resulted in diffuse, bilateral hemispheric distribution of maximum principal strains greater than zero in the brain, whereas impact to the model with adult cranial bone properties produced primarily focal, unilateral brain deformations. Maximum principal strains in excess of 0.15 have been associated

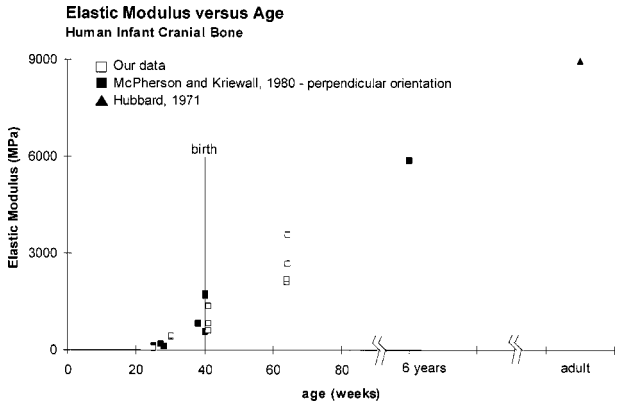

Fig. 6 Elastic modulus versus age for human infant cranial bone. Human data obtained in the current study shows agreement with the literature for quasi-static three-point bending.

with functional failure of the neural and vascular tissues [13,14]. Although further research is necessary to describe the complex three-dimensional geometry and properties of the infant head more accurately, these results in an idealized finite element model of a one-month-old infant support the hypothesis that impact loading, commonly associated with focal brain injury in a stiffer adult braincase [15], may produce diffuse injury in the compliant braincase of the infant.

Discussion

The goal of our study was to define the age-dependent mechanical behavior of the skull. Therefore, a simplified material model was assumed in which cranial bone and sutures are homogeneous, Hookean elastic materials capable of sustaining yield before failure. Care was taken to minimize the effects of anisotropy and inhomogeneity in all studies by consistently harvesting specimens from the same location and orientation across all subjects, and the effects of any minor variation in sample orientation was neglected during data analysis. Although specimens had a slight initial curvature over the span, the error caused by the initial curvature of each specimen was considered negligible for data analysis [1].

The important limitation of our experimental study was that porcine skull may not be an adequate model for human skull. Dobbing and colleagues [16,17] compared human central nervous system (CNS) development with several other species to develop an interspecies CNS scaling relationship and determined that during the first decade of human life, months of life in a human were roughly comparable to weeks in a pig. Although this scaling relation is for the CNS, we have adopted it for our porcine skull studies, in the absence of any other evidence regarding interspecies scaling. Thus, as a first approximation, and a 2–3-day-old pig correlates roughly with a less than one-month-old human newborn. This age-scaling assumption is supported in the next section by comparing human and porcine results.

Human Infant Cranial Bone. McPherson and Kriewall published a series of papers characterizing the elastic modulus of fetal parietal bone in three-point bending at a quasi-static loading rate [1–3]. Their results demonstrate a significant variation in the elastic modulus due to the orientation of clearly visible fibers within the bending specimen. Test specimens in McPherson's study were carefully prepared so the fibers were oriented parallel or perpendicular to the long axis of the specimen. In our study, all of the human and porcine bending samples were oriented with the fibers perpendicular to the long axis of the bending specimen. When compared with McPherson's data for perpendicularly oriented fibers, our data agree well with their published results (Fig. 6).

Between birth and six months of age, the single layer of cortical bone that forms the newborn's skull begins to differentiate structurally into the composite sandwich structure of the mature skull. In our six-month-old human subject (#4 in Table 1), the fibers in the parietal bone were not visible, and differentiation of the skull into its cortical and cancellous bony sandwich structure was clearly evident. In Figs. 4(*a*)–(*c*), structural differentiation of the cranial bone between birth and six months corresponds to an increase in the rupture modulus, elastic modulus, and energy absorbed to failure. Studies by Kriewall have determined that the ash content of term infant cranial bone is not significantly different from mature, composite cranial bone [2]. Kriewall concluded that structural differentiation, rather than ash content, most likely accounts for the increase in the elastic modulus of cranial bone with increasing age.

We hypothesize that the structural differentiation of cranial bone might also account for the increase in rupture modulus and energy absorbed to failure we observed in our tests. Mature cranial bone may be idealized as an engineering sandwich structure, with a low-density core surrounded by stiff skins [18]. Merely by increasing skull thickness, the diploë layer of the adult skull serves to increase its bending strength compared to the immature skull. In addition, because the diploë also stiffens the sandwich structure, it also enhances the skull's energy absorbing properties. The increased flexural strength provided by the cortical skin material and the energy absorbing capability of the thicker structure make the cranial bone of the mature skull a lightweight, efficient structure for carrying external loads in bending. We conclude that the structural properties of the developing skull are the most important factors in determining its overall mechanical response to external loads.

Although our study of human cranial bone was limited to a very small number of specimens, our results show good agreement with the few published data. However, the sparse mechanical data currently in the literature do not include any studies on the mechanical response of pediatric cranial sutures, and the rate dependence or failure criteria of pediatric cranial bone and suture. The use of a porcine infant animal model greatly extends the scope of our mechanical investigations to study these factors.

Porcine Infant Cranial Bone and Suture. One of the important findings in our porcine animal model is that the elastic modulus, rupture modulus, and energy absorbed to failure of porcine infant cranial bone are similar to that of the human infant in three-point bending (Figs. 7(*a*)–(*c*)). Two other important findings in our study are the comparative properties between cranial bone and suture in the infant, and the rate-dependence of those tissues. For the remainder of this discussion, we will assume that all of the properties of infant cranial bone and suture from the human and pig are similar, and conclusions drawn from our porcine data are valid for the human skull.

Pediatric Skull. Pediatric cranial bone is composed of cartilaginous matrix upon which stiff hydroxyapetite crystals are deposited to form dense cortical bone. We observed little or no cancellous diploë layer present in the cross section of bone from 2–3-day-old pigs. Pediatric sutures are patent, membranous butt joints between adjacent, developing bony plates.

The current study demonstrated significant differences between infant porcine cranial bone and suture for the elastic modulus, yield strain and ultimate strain, regardless of loading rate. Bone is significantly stiffer than suture, and yields and fails at strains significantly lower than suture. This is an important result because structural injury models of the infant head must include the hinge-like behavior of the immature sutures. Furthermore, the energy absorbed to failure, yield stress, and failure stress (or rupture modulus) of cranial bone and suture are not significantly different, regardless of loading rate.

Currently there are no data in the literature that characterize the effect of loading rate on the mechanical properties of infant cranial bone. Pediatric cranial bone is essentially cortical bone, and if ash content varies little with development of the skull, it is rea-

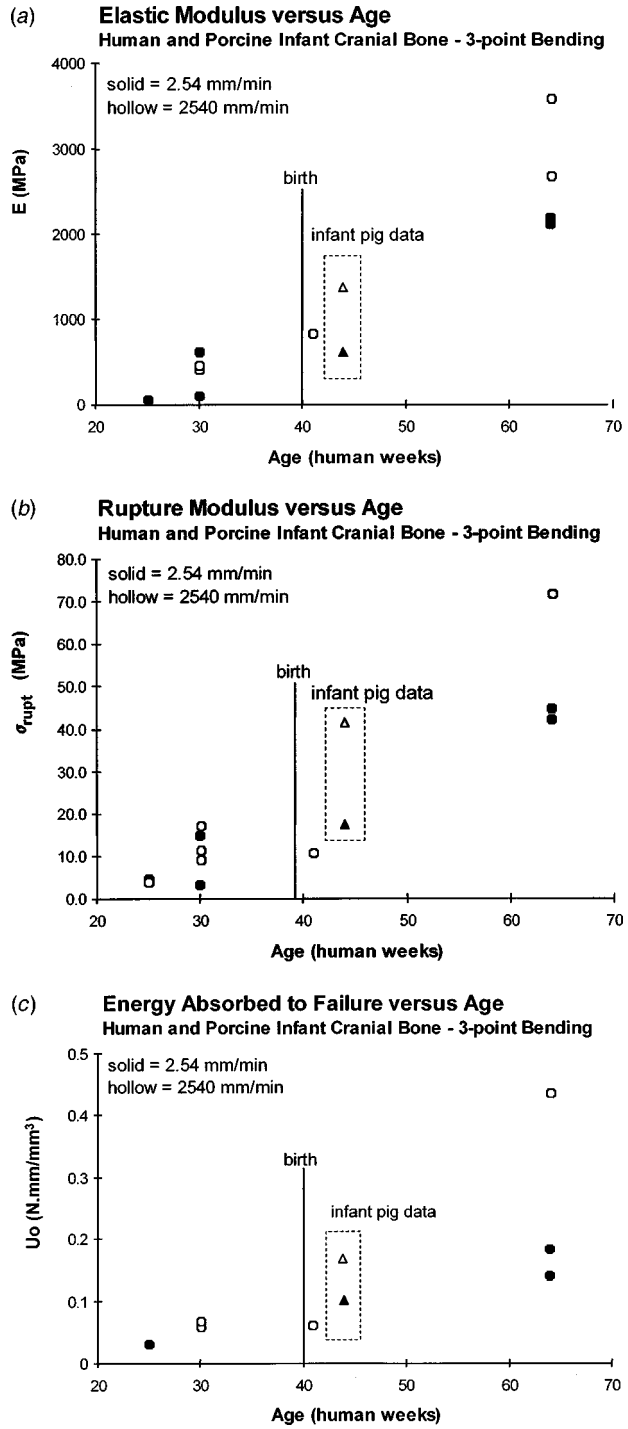

Fig. 7 (*a*) **Elastic modulus of porcine and human infant cranial bone determined from three-point bending tests;** (*b*) **rupture modulus of porcine and human infant cranial bone;** (*c*) **energy absorbed to failure of porcine and human infant cranial bone; slow rate** (**2.54 mm/min**) **and fast rate** (**2540 mm/min**)

sonable to compare our infant porcine data with previously published investigations of the rate-dependent mechanical behavior of adult human cranial cortical bone. Wood tested human cranial cortical bone in tension without the diploë layer and reported, as functions of increasing loading rate, increases in the elastic modulus and ultimate stress, a decrease in the ultimate strain, and no significant rate-dependent effect on energy absorbed to failure [19]. Our bending tests of infant porcine cranial bone show significant rate-dependent increases in rupture modulus and elastic modulus, but not in energy absorbed to failure. We conclude that porcine infant cranial bone exhibits rate-dependent behavior similar to adult human cortical bone.

Although their rate-dependent behavior is similar, the magnitude of porcine infant cranial bone mechanical properties differ considerably from those of adult human cortical bone. The elastic modulus for human neonatal parietal bone ranges between 120 and 4240 MPa in quasi-static three-point bending ([1] and current study), and porcine cranial bone ranges between 615 and 809 MPa in quasi-static (2.54 mm/min) three-point bending and tension, respectively. Wood reported a quasi-static elastic modulus of adult cortical bone in tension of ≈12,000 MPa [19]. Likewise, the ultimate stress and ultimate strain for pediatric cranial bone in quasi-static tension are 10.5 MPa and 0.034 mm/mm, respectively, as compared to Wood's values of ≈70 MPa and ≈0.007 mm/mm. The differences between pediatric bone and adult cortical bone may be due to incomplete calcification or interspecies differences.

Pediatric Suture. Currently there are no data in the literature regarding the rate-dependent mechanical properties of pediatric sutures. Our study has also shown that pediatric sutures exhibit rate-dependent mechanical behavior. In bending, suture tissue shows significant rate-dependent increases in rupture modulus and elastic modulus, but no significant rate-dependent increase in energy absorbed to failure. We conclude that the suture of the infant skull does not demonstrate enhanced ability to absorb energy during high rate loading.

The immature suture is composed of a series of periosteal and endosteal membranes spanning the gap between adjacent bony plates of the pediatric skull. In bending and tension, failure of the suture was caused by a separation of the membrane from the adjacent bone, and not a rupture of the membrane itself. We conclude that significant differences exist between the mechanical properties of immature cranial bone and suture, and these distinctions must be included in a structural injury model of the infant head.

Adult Cranial Bone and Sutures. Adult human cranial bone resembles a classical engineering sandwich structure composed of stiff facings of cortical bone (the inner and outer tables) and a compliant, lightweight core of cancellous bone (the diploë). Adult cranial sutures are the highly complex structures joining the bones of the skull that are composed of interdigitated edges of adjacent cranial bone spanned by collagenous fibers.

As a stiff functional unit, the cranial bones and sutures serve to protect the brain from impact injury. Sutures have been tested in bending [20,21] and in pendulum impact tests to determine the mechanical properties of the joints in the skull. Jaslow demonstrated that frontoparietal sutures absorb more energy during impact than adjacent cranial bone, and hypothesized that the presence of collagen within the suture and the highly irregular surface created during failure are thought to provide the suture with higher energy absorbing capabilities than bone [21]. In support of this theory, collagen has been shown to absorb at least 100 times more energy than bone per unit volume of tissue [22], and examination of fracture surfaces of cranial bone and suture indicate that the fracture surface of the suture is much more irregular than the planar fracture surfaces of the bone ([21]; our observations). Together, the present study and previous data [8,20,21] support the concept that the sutures in the adult skull may function as shock absorbers during impact loading of the skull, while bone may carry and distribute the load.

Adult human cranial bone and its individual components have been tested in tension [9,19,23], bending [8], compression [9,23,24] and simple shear [9] in order to characterize the mechanical response of the skull to traumatic loads. By combining the human and porcine skull data from the current study with the data in the literature, the age-dependent properties of the skull

may be defined. The elastic modulus of composite human cranial bone in bending increases from ≤1000 (quasi-static) to 1371 (dynamic) MPa at birth to ≈8000 MPa at maturity [8]. The quasi-static ultimate stress of cranial bone in tension increases from 10 Mpa (porcine) at birth to 43 [9] to 70 MPa [23] at maturity. The quasi-static ultimate strain in tension decreases from .034 mm/mm (porcine) at birth to ≈0.0052 mm/mm [8] at maturity. For the adult cortical bone layer only, Wood reported an elastic modulus of 12,000 MPa in tension [19]. Because mature sutures have properties similar to adult cranial bone [20], the elastic modulus and ultimate stress of sutures increase from ≈200 MPa (porcine) and 7 MPa (porcine) respectively at birth to the values for adult cranial bone as previously stated.

Conclusion

We have shown that the elastic modulus and the rupture modulus of infant cranial bone and suture increase significantly with loading rate but do not approach adult values. Most importantly, the energy absorbed to failure in each of the pediatric tissues does not change significantly with loading rate. The energy absorbed to failure for mature cranial sutures, as reported by Jaslow, is 0.498 $N \cdot mm/mm^3$ [21] compared with 0.1737 $N \cdot mm/mm^3$ for the infant porcine cranial sutures at the fast loading rate (2540 mm/min). Jaslow has also demonstrated that sutures absorb significantly more energy during impact than cranial bone, regardless of degree of interdigitation, confirming the shock absorbing role of the sutures in the skull [21]. We conclude that the shock absorbing capabilities of the cranial suture are not present in the infant.

To summarize, the elastic modulus, ultimate stress, and energy absorbed to failure increase, and the ultimate strain decreases with age for cranial bone. Likewise, the elastic modulus, ultimate stress, and energy absorbed to failure increase with age for sutures. A thin, pliant skull and patent sutures predispose the head of the newborn to large shape changes during external loading. These structural features are necessary during birth, where quasi-static head molding allows the passage of the head through the birth canal with minimal trauma. However, these same structural features leave the skull of the newborn with little ability to resist and absorb the large energies associated with traumatic loading. As calcification and differentiation of the skull take place, the infant skull begins to gain the necessary material and structural adaptations to protect the brain from trauma. The properties presented in this communication for infant skull and suture are necessary to predict the unique mechanical response of the pediatric skull to traumatic loads associated with head injury and, thus, is a first step in identifying head injury thresholds for children.

Acknowledgments

The authors wish to thank Dr. Alex Radin for his assistance with the Instron experiments, Drs. Bill Armstead and Lucy Rorke for providing infant porcine and human skull samples, respectively, Dr. Steve Kurtz for his expertise in the finite element analysis, and Failure Analysis and Associates for generously providing computer time for the simulations. The research was supported by a grant from the Center for Injury Research and Prevention, at the Centers for Disease Control, and by the University of Pennsylvania.

References

[1] McPherson, G. K., and Kriewall, T. J., 1980, ''The Elastic Modulus of Fetal Cranial Bone: A First Step Towards an Understanding of the Biomechanics of Fetal Head Molding,'' J. Biomech., **13**, pp. 9–16.
[2] Kriewall, T. K., et al., 1981, ''Bending Properties and Ash Content of Fetal Cranial Bone,'' J. Biomech., **14**, pp. 73–79.
[3] Kriewall, T. J., 1982, ''Structural, Mechanical, and Material Properties of Fetal Cranial Bone,'' Am. J. Obstet. Gynecol., **143**, pp. 707–714.
[4] Dejeammes, M., et al., 1984, ''Exploration of Biomechanical Data Towards a Better Evaluation of Tolerance for Children Involved in Automotive Accidents,'' SAE 840530 pp. 427–440.
[5] Duhaime, A. C., et al., 1987, ''The Shaken Baby Syndrome—A Clinical Pathological, and Biomechanical Study,'' J. Neurosurg., **66**, pp. 409–415.
[6] Stürtz, G., 1980, ''Biomechanical Data of Children,'' SAE Paper No. 801313.
[7] Mohan, D., Bowman, B. M., Snyder, R. G., and Fourst, D. R., 1979, ''A Biomechanical Analysis of Head Impact Injuries to Children,'' ASME J. Biomech. Eng., **101**, pp. 250–260.
[8] Hubbard, R. P., 1971, ''Flexure of Layered Cranial Bone,'' J. Biomech., **4**, pp. 251–263.
[9] McElhaney, J. H., et al., 1970, ''Mechanical Properties of Cranial Bone,'' J. Biomech., **3**, pp. 495–511.
[10] Thibault, K. L., and Margulies, S. S., 1998, ''Age-Dependent Material Properties of Porcine Cerebrum: Effect on Pediatric Inertial Head Injury Criteria,'' J. Biomech., **31**, pp. 1119–1126.
[11] Timoshenko, S. P., and Goodier, J. N., 1951, *Theory of Elasticity*, McGraw-Hill, New York.
[12] Datsko, J., 1986, ''Solid Materials,'' in: Shigley J. E., and Mischke, C. R., eds., *Standard Handbook of Machine Design*, McGraw-Hill, New York, Chap. 7.
[13] Margulies, S. S., Thibault, L. E., and Gennarelli, T. A., 1990, ''Physical Model Simulations of Brain Injury in the Primate,'' J. Biomech., **23**, pp. 823–836.
[14] Shreiber, D. I., Bain, A. C., and Meaney, D., 1997, ''In Vivo Thresholds for Mechanical Injury to the Blood–Brain Barrier,'' *Proc. 41st Stapp Car Crash Conference*, pp. 277–291.
[15] Gennarelli, T. A., and Meaney, D. F., 1996, ''Primary Head Injury Mechanisms,'' in: *Neurosurgery*, **2**, Wiekens, B., ed., McGraw-Hill, New York, pp. 2611–2621.
[16] Dickerson, J. W. T., and Dobbing, J., 1966, ''Prenatal and Postnatal Growth and Development of the Central Nervous System of the Pig,'' Proc. R. Soc. London, Ser. B, **166**, pp. 384–395.
[17] Dobbing, J., 1964, ''The Later Development of the Brain and Its Vulnerability,'' in: *Scientific Foundations of Paediatrics*, Davis, J. A., and Dobbings, J., eds., Heinemann Medical, London.
[18] Johnson, A. F., and Sims, G. D., 1986, ''Mechanical Properties and Design of Sandwich Materials,'' Composites, **17**, No. 4, pp. 321–328.
[19] Wood, J. L., 1971, ''Dynamic Response of Human Cranial Bone,'' J. Biomech., **4**, pp. 1–12.
[20] Hubbard, R. P., et al., 1971, ''Flexure of Cranial Sutures,'' J. Biomech., **4**, pp. 491–496.
[21] Jaslow, C. R., 1990, ''Mechanical Properties of Cranial Sutures,'' J. Biomech., **23**, No. 4, pp. 313–321.
[22] Wainwright, S. A., et al., 1976, *Mechanical Design of Organisms*, Princeton University Press, Princeton, NJ.
[23] Evans, F. G., and Lissner, H. R., 1957, ''Tensile and Compressive Strength of Human Parietal Bone,'' J. Appl. Physiol., **10**, pp. 493–497.
[24] Melvin, J. W., et al., 1969, ''The Mechanical Behavior of the Diploë Layer of the Human Skull in Compression,'' *Development in Mechanics: Proc. Midwestern Mechanics Conference*, **5**, pp. 811–818.